metals

MDPI

Article

Magnetostructural Transformation and Magnetocaloric Properties of $(Ni_{37.5}Co_{12.5}Mn_{35}Ti_{15})_{100-x}B_x$ (x = 0.0 and 0.4) Melt-Spun Ribbons

Mauricio López-Cruz [1,*], Rastislav Varga [2] and José Luis Sánchez Llamazares [1,*]

[1] Instituto Potosino de Investigación Científica y Tecnológica A.C., Camino a la Presa San José 2055, Col. Lomas 4ª, San Luis Potosí 78216, Mexico
[2] Centre for Progressive Materials, Technology, and Innovation Park, Pavol Jozef Safarik University in Kosice, 041 01 Kosice, Slovakia; rastislav.varga@upjs.sk
* Correspondence: mauricio.lopez@ipicyt.edu.mx (M.L.-C.); jose.sanchez@ipicyt.edu.mx (J.L.S.L.)

Abstract: The effect of B-doping on the martensitic transformation (MT), microstructure, room temperature (RT) crystal structure, and magnetocaloric properties of a typical all-d-metal $Ni_{37.5}Co_{12.5}Mn_{35}Ti_{15}$ quaternary alloy was studied by synthesizing melt-spun ribbon samples of nominal composition $(Ni_{37.5}Co_{12.5}Mn_{35}Ti_{15})_{100-x}B_x$ with x = 0.0 and 0.4. For B-free samples, SEM images show a grain-oriented microstructure formed by the columnar in shape-elongated grains with their major axis oriented along the thermal gradient during solidification. By contrast, the B-doped samples show smaller grains whose orientation tends to be perpendicular to the contact surface with the copper wheel. For all samples, austenite (AST) and martensite (MST) phases exhibited a cubic B2-type and 5M monoclinic crystal structure, respectively. The martensitic transition temperature (T_M) and the Curie temperature of the austenite phase ($T_C{}^A$) were reduced from 295 K to 253 K and 333 K to 276 K, respectively, with the addition of B. The effect of thermal annealing for different times (from 30 min to 4 h) at 1073 K was studied. Thermal annealing increases the martensitic transformation temperature, whereas $T_C{}^A$ remains unchanged. The maximum magnetic field-induced entropy changes $|\Delta S_T|^{max}$ for B-doped samples were around 4.5 J kg^{-1} K^{-1} and 4.7 J kg^{-1} K^{-1} for as-solidified and annealed samples (1073 K–4 h), respectively, compared to that found for the undoped samples (i.e., ΔS_T = 16 J kg^{-1} K^{-1}). However, the entropy reduction is accompanied by an increase in the full width at half-maximum of the $\Delta S_T(T)$ curve.

Keywords: all-d-metal Ni-Co-Mn-Ti-B ribbons; martensitic transformation; magnetic entropy change

check for updates

Citation: López-Cruz, M.; Varga, R.; Sánchez Llamazares, J.L. Magnetostructural Transformation and Magnetocaloric Properties of $(Ni_{37.5}Co_{12.5}Mn_{35}Ti_{15})_{100-x}B_x$ (x = 0.0 and 0.4) Melt-Spun Ribbons. *Metals* **2024**, *14*, 216. https://doi.org/10.3390/met14020216

Academic Editors: Aphrodite Ktena and Ian Baker

Received: 18 December 2023
Revised: 18 January 2024
Accepted: 7 February 2024
Published: 9 February 2024

Copyright: © 2024 by the authors. Licensee MDPI, Basel, Switzerland. This article is an open access article distributed under the terms and conditions of the Creative Commons Attribution (CC BY) license (https://creativecommons.org/licenses/by/4.0/).

1. Introduction

Motivated by the search for new, more energy-efficient, and environmentally friendly solid-state-based refrigeration technologies, magnetic refrigeration has received considerable attention over the last 25 years [1]. This technology is based on the magnetocaloric effect (MCE), a magneto-thermal phenomenon quantitatively characterized by the thermal dependence of the change in the temperature $\Delta T_{ad}(T)$ or magnetic field-induced entropy change $\Delta S_T(T)$ under adiabatic and isothermal conditions, respectively, linked to a second or first-order magnetic transition when the material is subject to a magnetic field change $\mu_o \Delta H$ [2–6]. In this sense, in most of the efforts to develop magnetic refrigerants that are able to be used as working substances at room temperature (RT), magnetic refrigerators have focused on magnetocaloric material systems exhibiting a giant MCE linked to first-order magnetic transitions (FOMT). The term "giant magnetocaloric effect" (GMCE) refers to the sizeable magnetic-field-driven change in magnetic entropy and adiabatic temperature changes that a magnetically ordered material experiences in the temperature range at which it undergoes a first-order magnetoelastic or magnetostructural transition. Among the material families showing GMCE, (Ni, Mn)-based Heusler-type alloys derived from ternary Ni-

Mn-X systems, X = Ga, In, Sn, and Sb have been the focus of extensive research over the last 20 years since in some alloys a remarkable magnetocaloric effect has been experimentally determined [7–11]. However, the brittleness of these alloy systems is one of the essential drawbacks of their practical utilization in cooling devices and any other application. In this regard, the more recently discovered all-*d*-metal-type alloys in the Ni-Co-Mn-Ti system combine a giant magnetocaloric effect with excellent mechanical properties [12,13]. Wei et al. were the first to report the magnetostructural transformation in bulk $Ni_{50-x}Co_xMn_{35}Ti_{15}$ with x = 8.0 and 9.5 [14]. They demonstrated that martensitic transformation takes place from a high-temperature ferromagnetic (FM) cubic B2-type austenite to a low-temperature weak-magnetic monoclinic martensite (space group *p2/m*) [14,15]. However, the maximum field-induced entropy changes $\Delta S_T{}^{max}$ reported for bulk were moderate (10 J kg^{-1} K^{-1} and 18 J kg^{-1} K^{-1} at 2 T and 5 T, respectively) [14,15]. Nevertheless, some years later, Neves Bez et al. demonstrated the efficacy of the melt-spinning technique to optimize the magnetocaloric effect [16]: $\Delta S_T{}^{max}$ values at $\mu_o\Delta H$ = 2 T ($\Delta S_T{}^{max}$ = 27.2 J kg^{-1} K^{-1}) around room temperature were found in as-solidified $Ni_{37.5}Co_{12.5}Mn_{35}Ti_{15}$ ribbons [16].

Alloying elements, such as Fe [17], Cu [16,18,19], V [20], Cr [21], and B [12,22], have been added to Ni-Co-Mn-Ti alloys to tune the temperature of the structural transition or to improve the mechanical and magnetocaloric properties. Due to its small atomic radio and depending on the amount added, B is an element that may occupy interstitial or substitutional sites in Heusler-type Ni-Mn-X alloys [23–26]. Recently, Zhang et al. studied the effect of B on the thermal hysteresis ΔT_{hyst} of the magnetostructural transition and magnetocaloric properties of $Ni_{36.5}Co_{13.5}Mn_{35}Ti_{15}$ alloys [22]. They demonstrated that interstitial B in the $(Ni_{36.5}Co_{13.5}Mn_{35}Ti_{15})_{99.6}B_{0.4}$ alloy significantly reduces ΔT_{hyst} (~4.4 K) and simultaneously increases $\Delta S_T{}^{max}$ from 3.8 J kg^{-1} K^{-1} (9.7 J kg^{-1} K^{-1}) to ~11 J kg^{-1} K^{-1} (24.3 J kg^{-1} K^{-1}) for a magnetic field change of 2 T (5 T). Likewise, Guan et al. reported improved mechanical properties with B-doping in $Ni_{37}Co_{13}Mn_{34}Ti_{16}$, which maintained a high value of $\Delta S_T{}^{max}$ (~40 J kg^{-1} K^{-1}) at a magnetic field of 7 T [12]. However, the extended thermal treatment of 1123 K for two days and 1173 K for six days was used for the alloys studied by Guan et al. [12] and Zhang et al. [22], respectively.

Guided by these previous works, we addressed the synthesis of melt-spun ribbons of $(Ni_{37.5}Co_{12.5}Mn_{35}Ti_{15})_{100-x}B_x$ alloys with x = 0.0 and 0.4 to assess the effect of B on the martensitic transformation and related magnetocaloric properties. The B-containing samples were also thermally annealed for 4 h at a moderate temperature of 1073 K to obtain preliminary information on how it affects the magnetostructural martensitic transformation temperature and related $\Delta S_T(T)$ curve.

2. Materials and Methods

The initial bulk alloys to prepare rapidly solidified melt-spun ribbon samples had a nominal composition $(Ni_{37.5}Co_{12.5}Mn_{35}Ti_{15})_{100-x}B_x$, with x = 0.0 and 0.4. The elements used to prepare them were 99.99% Ni (Alfa Aesar, Haverhill, MA, USA), 99.95% Co (Alfa Aesar), 99.9% Mn (Alfa Aesar), 99.99% Ti (Aldrich, St. Louis, MO, USA), and 99.4% B (Aldrich). Small pellets of 4 g were produced via arc melting under a highly pure argon atmosphere (99.999%) in a water-cooled copper crucible. Samples were flipped and remelted four times to ensure a good starting element mixture. An excess of Mn of 3 wt. % was added to both samples to compensate for the loss of this element by evaporation. The initial and final mass of the alloys prepared were the same.

Melt-spun ribbons were fabricated under a highly pure Ar atmosphere in an Edmund Bühler model SC melt-spinner system. Once molten, the alloys were ejected by applying an argon overpressure of 200 mbar onto the polished surface of a 200 mm diameter copper wheel rotating at a linear speed of 20 ms^{-1}. The as-solidified ribbon samples typically had the following physical dimensions: 1.0–1.5 mm width and 20 mm length. B-containing ribbon samples were sealed in vacuumed quartz ampoules to be thermally annealed at 1073 K for 4 h; thermal annealing (TA) ended with water quenching at 373 K for 20 min.

Hereafter, we focus on characterizing these three ribbon samples, referred to as x = 0.0 AS, x = 0.4 AS, and x = 0.4 TA, respectively.

X-ray diffraction (XRD) patterns were collected at room temperature in a high-resolution Rigaku Smartlab diffractometer (CuKα, λ = 1.54059 Å; $30^\circ \leq 2\theta \leq 90^\circ$, Rigaku Corporation, Tokyo, Japan). The main goal of XRD analyses was the determination of the phase constitution at room temperature for the ribbon samples studied.

Differential scanning calorimetry (DSC) curves were measured on a TA-DSC Q200 system (TA Instruments, New Castle, DE, USA) in the temperature interval 220 K–320 K at a heating and cooling temperature sweep rate of 10 K min^{-1}. The initial and final temperatures of the direct and reverse martensitic transition (M_S and M_f, and A_S and A_f, respectively) were determined by a simple extrapolation from the DSC and $M(T)^{5mT}$ curves. The thermal hysteresis ΔT_{hyst} of the magnetostructural transition was estimated as $\Delta T_{hyst} = A_f - M_S$.

Microstructural and semi-quantitative elemental chemical composition analyses were performed in an FEI QUANTA 250 SEM (FEI Company, Hillsboro, OR, USA) equipped with an energy dispersive spectroscopy (EDS) system from EDAX.

Magnetization measurements were conducted in a 9 T Quantum Design PPMS® Dynacool® system (Quantum Design, San Diego, CA, USA) using the vibrating sample magnetometry (VSM) option. The magnetic field was applied along the ribbon length to reduce the internal magnetic demagnetizing field. The thermal dependencies of the magnetization, the $M(T)$ curves, were measured under static magnetic fields of 5 mT, 2 T, and 5 T at a temperature range of 100–400 K with a temperature sweep rate of 1.5 K min^{-1} following zero-field-cooling (ZFC) and field-cooling (FC) regimens.

3. Results

Figure 1 compares the typical granular microstructure exhibited by as-solidified (AS) ribbons on the contact (CS, Figure 1a,b) and non-contact (NCS, Figure 1c,d) surfaces, and for the cross-section (Figure 1e,f). Columnar-shaped grains grow along the parallel direction to the thermal gradient during solidification, i.e., the longer axis of grains tends to orient perpendicular to both ribbon surfaces (see Figure 1e,f). The cross-sectional views denote this reduction in the average thickness of B-doped ribbons (~20 μm) compared to B-free samples (~38 μm). Also, a slight but perceptible increase in the average grain size was observed, suggesting that B promotes grain growth. As the pictures show, the B-free sample shows grains with and without martensitic domains, denoting the coexistence of austenite and martensite. By contrast, in the B-doped sample, no martensitic domains appeared. The latter is consistent with the temperature shift of the martensitic transformation with B addition, as the DSC and low-field $M(T)$ curves show (see below). EDS semi-quantitative analyses were performed in several selected zones on the CS and NCS (the typical spectra recorded are shown in Figure S1 of the Supplementary Material file). From them, and not considering the B amount, the average elemental chemical compositions determined were as follows: $Ni_{35.6\pm1.2}Co_{12.1\pm1.0}Mn_{37.0\pm1.1}Ti_{15.3\pm0.6}$ for x = 0.0 AS, $Ni_{35.9\pm1.3}Co_{10.7\pm1.0}Mn_{37.8\pm1.1}Ti_{15.6\pm0.5}$ for x = 0.4 AS, and $Ni_{35.9\pm1.2}Co_{10.4\pm1.0}Mn_{37.5\pm1.2}Ti_{16.2\pm0.6}$ for x = 0.4 TA. Within the error in the determination, the semi-quantitatively determined composition is close to that of $Ni_{37.5}Co_{12.5}Mn_{35}Ti_{15}$.

Figures 2 and 3a present the RT XRD patterns and DSC scans for as-solidified (AS) B-free and B-doped samples and the B-doped thermally annealed one. XRD patterns corresponding to the x = 0.0 AS sample reveal the coexistence of a cubic B2-type austenite and a 5-modulated (5M) monoclinic martensite phase. This is consistent with what was reported in the refs. [14,15], and agrees with the calorimetry curves shown in Figure 3a since a martensitic transition took place around RT, and, therefore, a mixture of both phases coexisted in the sample. However, the patterns for the B-doped samples correspond to a pure B2-type austenite since, as Figure 3a shows, the martensitic transformation appeared below room temperature. In earlier reports, austenite showed a B2-type crystal structure [12,17,18,27]. The lattice parameters were determined using the equation

$\frac{1}{d^2} = \frac{h^2+k^2+l^2}{a^2}$ and $\frac{1}{d^2} = \frac{1}{sin^2\beta}\cdot\left(\frac{h^2}{a^2} + \frac{k^2 sin^2\beta}{b^2} + \frac{l^2}{c^2} - \frac{2hl\cdot cos\beta}{ac}\right)$ for cubic and monoclinic systems, respectively. They are summarized in Table 1. As previously stated, if the B amount does not exceed a critical value, B atoms occupy interstitial sites in the crystal structure, increasing the cell volume [22]. This explains the increased cell volume of the B-doped ribbon samples compared to the B-free ones. However, as the samples were prepared using a non-equilibrium technique such as melt spinning, they always showed some local crystalline disorder, which tended to enlarge the cell volume. Notice that the cell volume of austenite in B-doped as-solidified ribbon samples is higher than that of the B-free ones. However, partial local disorder decreases in interstitially doped samples after the thermal annealing with a consequent cell volume reduction.

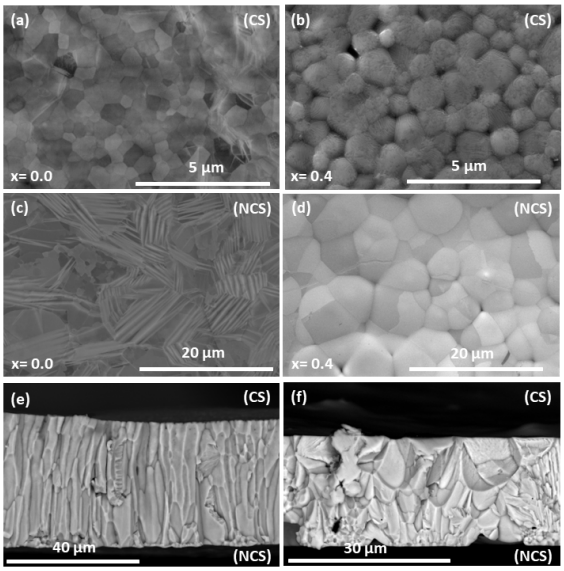


Figure 1. SEM micrograph of the typical microstructure exhibited by as-solidified $(Ni_{37.5}Co_{12.5}Mn_{35}Ti_{15})_{100-x}B_x$ ribbons with x = 0.0 and 0.4 at the contact (**a**,**b**) and non-contact surfaces (**c**,**d**) with the copper wheel, and at the cross-section (**e**,**f**).

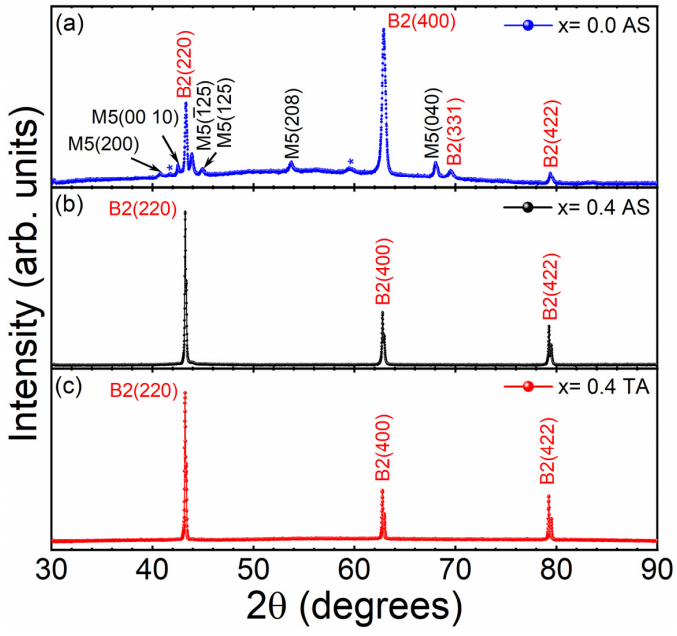


Figure 2. Room temperature XRD patterns for $(Ni_{37.5}Co_{12.5}Mn_{35}Ti_{15})_{100-x}B_x$ ribbon samples: x = 0.0 AS (**a**), x = 0.4 AS (**b**), and x = 0.4 TA (**c**). The asterisk indicates a minor unidentified peak (at 2θ = 59.3°).

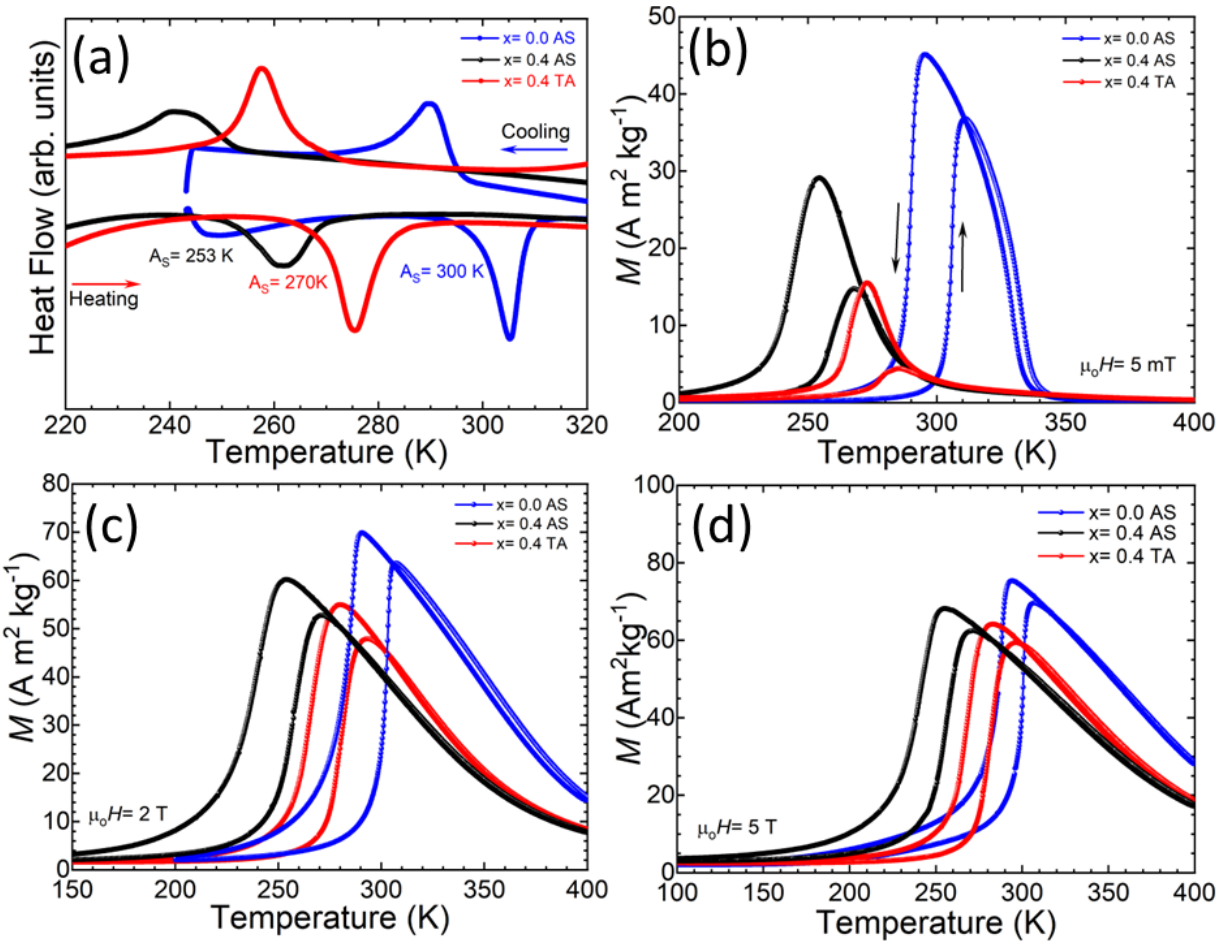


Figure 3. DSC curves (**a**), and ZFC and FC M(T) curves at 5 mT (**b**), 2 T (**c**), and 5 T (**d**) for x = 0.0 AS (blue line), x = 0.4 AS (black line), and x = 0.4 TA (red line) samples.

Table 1. Unit cell parameters and cell volume obtained for the $(Ni_{37.5}Co_{12.5}Mn_{35}Ti_{15})_{100-x}B_x$ ribbon samples studied (x = 0.0 AS, x = 0.4 AS, and x = 0.4 TA).

Sample	Structure	Cell Parameters (Å)			Angles (°)	Cell Volume (Å)^3
		a	*b*	*c*		
x = 0.0 AS	Monoclinic	4.428	5.508	21.30	α = γ = 90 β = 94.1386	518.251
	Cubic	5.901	5.901	5.901	α = β = γ = 90°	205.542
x = 0.4 AS	Cubic	5.915	5.914	5.914	α = β = γ = 90°	206.935
x = 0.4 TA	Cubic	5.699	5.699	5.699	α = β = γ = 90°	185.112

Figure 3a compares the DSC curves measured on heating and cooling for x = 0.0 AS (blue line), x = 0.4 AS (black line), and x = 0.4 TA (red line) samples. All samples show exothermic and endothermic peaks corresponding to the direct and reverse martensitic transformation. Table 2 lists the characteristic temperatures (A_S, A_f, M_S, and M_f) determined via simple extrapolation from the DSC and $M(T)$ curves measured at 5 mT and the thermal hysteresis of the transformation (ΔT_{hyst}). The DSC curves show that the martensitic transition temperature (T_M), defined as $T_M = (A_S + A_f + M_S + M_f)/2$, decreased by around 42 K with the addition of B. This behavior contrasts with previous works on bulk samples that show a temperature increase in the martensitic transition temperature with the increase in the B content [12,22]. In addition, a T_M increase appears after the thermal annealing at 1073 K for 4 h. This shift to higher temperatures of the magnetostructural transition temperature is consistent with previous results [28].

Table 2. A_S, A_f, M_S, M_f, ΔT_{hyst}, and $T_C{}^A$ parameters obtained from DSC and $M(T)^{5mT}$ curves for the $(Ni_{37.5}Co_{12.5}Mn_{35}Ti_{15})_{100-x}B_x$ ribbon samples studied (x = 0.0 AS, x = 0.4 AS, and x = 0.4 TA).

DSC						
Sample	**AS (K)**	**Af (K)**	**MS (K)**	**Mf (K)**	**ΔThyst (K)**	**TC^A (K)**
x = 0.0 AS	300	309	295	281	14	×
x = 0.4 AS	253	270	253	233	17	×
x = 0.4 TA	270	282	265	251	17	×
$M(T)^{5\,mT}$						
x = 0.0 AS	303	309	292	286	17	333
x = 0.4 AS	253	268	254	235	14	276
x = 0.4 TA	272	283	272	260	11	290

Figure 3 shows the ZFC and FC $M(T)$ curves for x = 0.0 AS (blue line), x = 0.4 AS (black line), and x = 0.4 TA (red line) samples measured under static magnetic fields ($\mu_o H$) of 5 mT (Figure 3b), 2 T (Figure 3c) and 5 T (Figure 3d). Notice that, with B-doping, the Curie temperature of austenite phase $T_C{}^A$ (determined from the minimum of the $dM/dT(T)$ curve at 5 mT) decreases at around 57 K. Then, the temperature difference between the magnetostructural (T_M) and magnetic transition of austenite ($T_C{}^A$) significantly reduces, making it difficult to estimate $T_C{}^A$ for x = 0.4 AS and TA samples. In addition, the magnetization change ΔM across the first-order transition becomes lower. It can be noticed that at 2 T and 5 T, ΔM decreased from 64 $Am^2\ kg^{-1}$ (x = 0.0 AS) to 53 $Am^2 kg^{-1}$ (x = 0.4 AS) (see Figure 3c) and from 70 $Am^2\ kg^{-1}$ (x = 0.0 AS) to 63 $Am^2\ kg^{-1}$ (x = 0.4 AS) (see Figure 3d), respectively, (values that were roughly estimated from the respective $M(T)$ curves for the magnetostructural transition on heating). For the x = 0.4 TA samples, ΔM was further reduced to 45 $Am^2\ kg^{-1}$ and 59 $Am^2\ kg^{-1}$ at 2 T and 5 T, respectively, due to the shift to higher temperatures of the magnetostructural transformation (which further reduced the temperature difference with the magnetic transition of austenite).

To investigate the effect of B-doping on the magnetocaloric properties of these samples, sets of isofield $M(T)$ curves were measured on heating through the reverse martensitic transformation. Owing to the first-order nature of the magnetostructural phase transition, after one isofield $M(T)$ curve on heating was measured, the magnetic field was set to zero, and the sample was then cooled down at the zero fields well below M_f to complete the martensitic transformation, and then heated again to the starting measuring temperature to record the next $M(T)$ curve. The sets of isofield curves are shown in Figure S2 of the Supplementary Material file; each graph shows the starting and finishing temperature at which the $M(T)$ curves were measured. From these measurements, the magnetic field-induced entropy changed as a function of temperature; the $\Delta S_T(T)$ curves were estimated from the numerical integration of the Maxwell relation [29]. Figure 4a compares the $\Delta S_T(T)$ curves at a magnetic field change of 2 T for x = 0.0 AS, x = 0.4 AS, and x = 0.4 T samples. The peak, or maximum, entropy change value $|\Delta S_T|^{max}$ decreased with B-doping from 13.6 J kg^{-1} K^{-1} to 4.1 J kg^{-1} K^{-1} for a $\mu_o \Delta H$ = 2 T and from 24.7 J kg^{-1} K^{-1} to 12.3 J kg^{-1} K^{-1} for a $\mu_o \Delta H$ = 5 T; however, it can be noticed that the ΔST(T) curves become broader. This behavior agrees with the report in Ref. [30] for B-doped samples with ≥0.2 at.%. However, it contrasts with the reported by Guan et al. [12] since these authors reported that $|\Delta S_T|^{max}$ remains almost unchanged after doping. Our results also differ from those of Zhang et al. [22] because they demonstrate that through B-doping, $|\Delta S_T|^{max}$ increased from 3.8 J kg^{-1} K^{-1} to around 11 J kg^{-1} K^{-1} at $\mu_o \Delta H$ = 2 T and from 9.7 J kg^{-1} K^{-1} to 24.3 J kg^{-1} K^{-1} at a $\mu_o \Delta H$ = 5 T. As Table 3 shows, the thermal annealing increased the structural transition temperature and $|\Delta S_T|^{max}$ in the B-doped ribbons. Figure 4b depicts the temperature dependence of the magnetic hysteresis loss for a magnetic field change of 2 T (i.e., the $HL(T)$ graph). The HL values for each temperature were determined from the area between the isothermal magnetization curves on increasing the magnetic field to 2 T and decreasing it to zero. Figure S3 depicts the magnetization curves in the martensite-to-

austenite phase transition temperature interval measured for each sample. It is highlighted that, due to the first-order nature of the transition, for each temperature, the $M(\mu_o H)$ curves were measured following the proper thermomagnetic protocol. The average hysteresis loos value, <*HL*> value, was estimated from the *HL*(*T*) curve in the temperature interval given by the full-width at half maximum, $\delta T_{FWHM} = T_{hot} - T_{cold}$, of the $\Delta S_T(T)$ curve. As can be seen, the addition of B led to a decrease in <*HL*>. Table 3 summarizes the significant magnetocaloric properties through the AST-MST phase transition, including the refrigerant capacity (*RC*) values. *RC* is an important magnetocaloric parameter that measures the heat the material can transfer between hot and cold reservoirs if an ideal refrigeration cycle is considered. *RC* was estimated using the following criteria: (i) *RC*-1 = $|\Delta S_T|^{max} \times \delta T_{FWHM}$, where $\delta T_{FWHM} = T_{hot} - T_{cold}$; (ii) by calculating the area under the $\Delta S_T(T)$ curve between T_{hot} and T_{cold} (*RC*-2); and (iii) by maximizing the product $\Delta S_T \times \delta T$ below the $\Delta S_T(T)$ curve (*RC*-3; Wood and Potter criterion) [31]. The effective magnetic refrigeration capacity (RC_{eff}) at 2 T can be calculated by subtracting <*HL*> from the respective *RC* value.

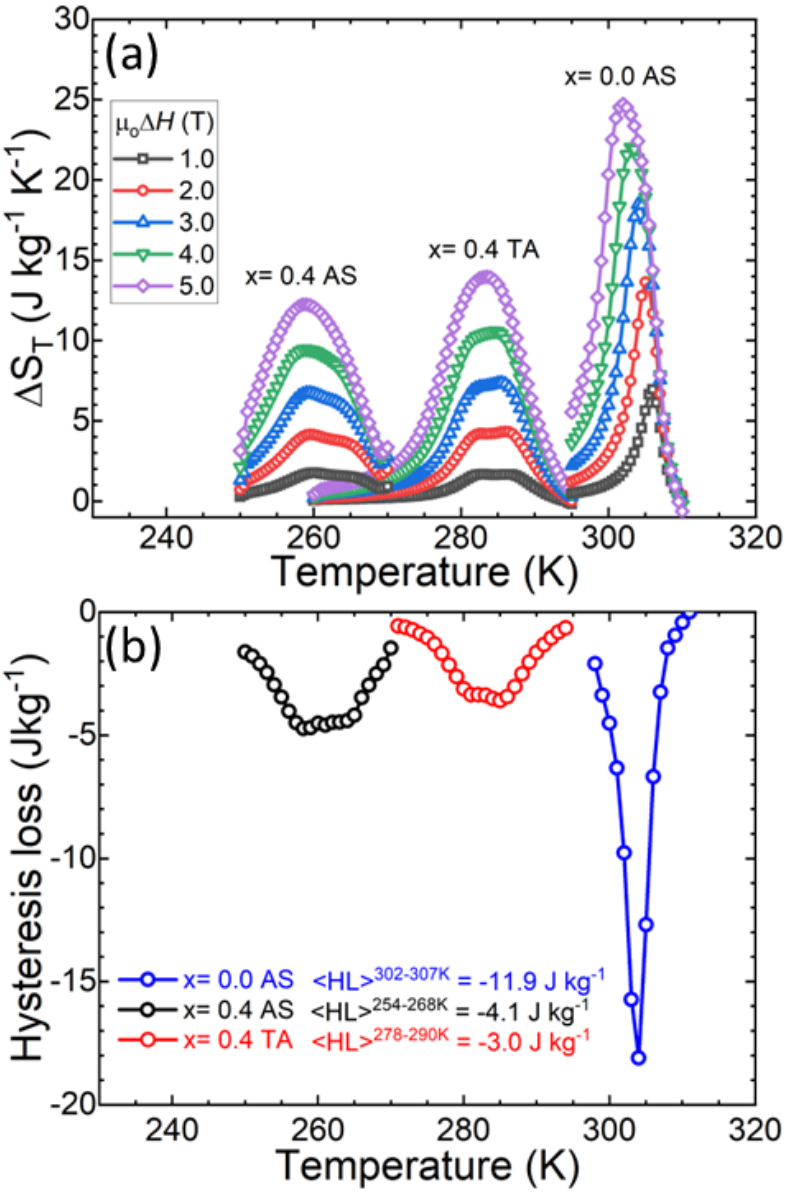


Figure 4. $\Delta S_T(T)$ curves at 1, 2, 3, 4, and 5 T (**a**) and *HL*(*T*) at 2 T (**b**) across the AFM-FM transition for x = 0.0 AS, x = 0.4 AS and x = 0.4 TA ribbon samples.

Table 3. $|\Delta S_T|^{max}$, *RC*-1, *RC*-2, *RC*-3, δT_{FWHM}, and δT^{RC-3}, through the AFM-FM martensitic transformation under magnetic field changes of 2 and 5 T, were linked to the MST-to-AST phase transition for the $(Ni_{37.5}Co_{12.5}Mn_{35}Ti_{15})_{100-x}B_x$ ribbon samples studied. <*HL*> represents the average value of the magnetic hysteresis loss at 2 T over δT_{FWHM}.

	***x* = 0.0 AS**		***x* = 0.4 AS**		***x* = 0.4 TA**	
	$\mu_o\Delta H$ = 2 T	**$\mu_o\Delta H$ = 5 T**	**$\mu_o\Delta H$ = 2 T**	**$\mu_o\Delta H$ = 5 T**	**$\mu_o\Delta H$ = 2 T**	**$\mu_o\Delta H$ = 5 T**
$\lvert\Delta S_T\rvert^{max}$ (J kg^{-1} K^{-1})	13.6	24.7	4.1	12.2	4.2	14.0
<*HL*> (J kg^{-1})	−12	×	−4.1	×	−3.0	×
RC-1 (J kg^{-1})	58	195	59	183	49	176
RC-2 (J kg^{-1})	47	163	48	150	43	144
T_{hot} (K)	307	306	268	266	290	289
T_{cold} (K)	303	298	254	252	278	276
δT_{FWHM} (K)	4	8	14	15	12	13
RC-3 (J kg^{-1})	29	105	31	97	29	92
δT^{RC-3} (K)	4.5	6	13	12	8	10
$T_{hot}{}^{RC-3}$ (K)	307	305	267	265	288	288
$T_{cold}{}^{RC-3}$ (K)	303	299	255	253	280	278

4. Conclusions

This work demonstrates how single-phase ribbon samples doped with interstitial B can be obtained in the Ni-Co-Mn-Ti system through rapid solidification using the melt-spinning technique, as confirmed using X-ray diffraction and thermomagnetic analysis curves. As in bulk samples, austenite exhibits a B2-type crystal structure. B-doping decreases the martensitic transformation temperature and the Curie temperature of austenite by around 42 K and 57 K, respectively; this radically differs from the reported for bulk alloys, demanding further study. Also, the maximum field-induced entropy change and thermal hysteresis reduce with the small amount of B added (0.4 at.%). Thermal annealing at a moderate temperature of 1073 K increases the magnetostructual transition temperature close to room temperature and does not reduce $\Delta S_T{}^{max}$ and the Curie temperature of austenite compared to the obtained as-solidified B-doped samples.

Supplementary Materials: The following supporting information can be downloaded at: https://www.mdpi.com/article/10.3390/met14020216/s1, Figure S1: Typical EDS spectra obtained for as-solidified $(Ni_{37.5}Co_{12.5}Mn_{35}Ti_{15})_{100-x}B_x$ melt-spun ribbons with x = 0.0 AS (a), x = 0.4 AS (b), and thermally annealed ribbons with x = 0.04 TA (c); Figure S2: Set of isofield $M(T)$ curves measured for heating $(Ni_{37.5}Co_{12.5}Mn_{35}Ti_{15})_{100-x}B_x$ ribbon samples: x = 0.0 AS (a), x = 0.4 AS (b), and x = 0.4 TA (c) (0.05 T $\leq \mu_o H \leq$ 2 T); Figure S3: Set of isothermal $M(\mu_o H)$ curves measured for increasing and removing the magnetic field through the MST-to-AST phase transition for $(Ni_{37.5}Co_{12.5}Mn_{35}Ti_{15})_{100-x}B_x$ ribbon samples: as-solidified (a), x = 0.0 (AS), x = 0.4 (AS) (b), and x = 0.4 (TA) (c). They were used to determine the thermal dependence of the magnetic hysteresis loss for each sample.

Author Contributions: Conceptualization, J.L.S.L.; methodology, M.L.-C.; data collection M.L.-C. and J.L.S.L.; software M.L.-C.; data analysis and interpretation M.L.-C., R.V., and J.L.S.L.; writing—original draft preparation, M.L.-C.; writing—review and editing, R.V. and J.L.S.L.; supervision, R.V. and J.L.S.L. All authors have read and agreed to the published version of the manuscript.

Funding: This work is supported by Laboratorio Nacional de Nanociencias y Nanotecnología (LINAN, IPICyT), SEP-CONAHCyT, México, funded this research, grant number CF-2023-I-2143, The Slovak Grant Agency APVV-160079 grant and VEGA 1/0180/23. M. López Cruz is grateful to CONAHCYT and SAIA for supporting his Ph.D. studies at IPICyT (scholarship number 831827) and at UPJS in Slovakia, respectively.

Data Availability Statement: The original contributions presented in the study are included in the article/supplementary material, further inquiries can be directed to the corresponding author/s.

Conflicts of Interest: The authors declare no conflicts of interest.

References

1. Tegus, O.; Brück, E.; Buschow, K.H.J.; de Boer, F.R. Transition-metal-based magnetic refrigerants for room-temperature applications. *Nature* **2002**, *415*, 150–152. [CrossRef]
2. Gschneidner, V.K.; Pecharsky, K.A., Jr. Magnetocaloric Materials. *Annu. Rev. Mater. Sci.* **2000**, *30*, 387–429. [CrossRef]
3. Pecharsky, V.K.; Gschneidner, K.A., Jr.; Pecharsky, A.O.; Tishin, A.M. Thermodynamics of the magnetocaloric effect. *Phys. Rev. B* **2001**, *64*, 144406. [CrossRef]
4. Shen, B.G.; Sun, J.R.; Hu, F.X.; Zhang, H.W.; Cheng, Z.H. Recent Progress in Exploring Magnetocaloric Materials. *Adv. Mater.* **2009**, *21*, 4545–4564. [CrossRef]
5. Kitanovski, A. Energy Applications of Magnetocaloric Materials. *Adv. Energy Mater.* **2020**, *10*, 1903741. [CrossRef]
6. Law, J.Y.; Moreno-Ramírez, L.M.; Díaz-García, Á.; Franco, V. Current perspective in magnetocaloric materials research. *J. Appl. Phys.* **2023**, *133*, 040903. [CrossRef]
7. Liu, J.; Gottschall, T.; Skokov, K.P.; Moore, J.D.; Gutfleisch, O. Giant magnetocaloric effect driven by structural transitions. *Nat. Mater.* **2012**, *11*, 620–626. [CrossRef]
8. Li, Z.; Zhang, Y.; Sánchez-Valdés, C.F.; Llamazares, J.L.S.; Esling, C.; Zhao, X.; Zuo, L. Giant magnetocaloric effect in melt-spun Ni-Mn-Ga ribbons with magneto-multistructural transformation. *Appl. Phys. Lett.* **2014**, *104*, 044101. [CrossRef]
9. Li, Z.; Li, Z.; Yang, J.; Yang, B.; Zhao, X.; Zuo, L. Large room temperature adiabatic temperature variation in a $Ni_{40}Co_8Mn_{42}Sn_{10}$ polycrystalline alloy. *Intermetallics* **2018**, *100*, 57–62. [CrossRef]
10. Li, Z.; Dong, S.; Li, Z.; Yang, B.; Liu, F.; Sánchez-Valdés, C.; Llamazares, J.S.; Zhang, Y.; Esling, C.; Zhao, X.; et al. Giant low-field magnetocaloric effect in Si alloyed Ni-Co-Mn-In alloys. *Scr. Mater.* **2018**, *159*, 113–118. [CrossRef]
11. Zhang, G.; Li, D.; Liu, C.; Li, Z.; Yang, B.; Yan, H.; Zhao, X.; Zuo, L. Giant low-field actuated caloric effects in a textured $Ni_{43}Mn_{47}Sn_{10}$ alloy. *Scr. Mater.* **2021**, *201*, 113947. [CrossRef]
12. Guan, Z.; Bai, J.; Zhang, Y.; Gu, J.; Morley, N.; Zhang, Y.; Esling, C.; Zhao, X.; Zuo, L. Ni-Co-Mn-Ti-B high performance multiferroic phase transformation material: Simultaneous modulation of mechanical properties and successive caloric effects by B doping. *Mater. Today Phys.* **2023**, *36*, 101183. [CrossRef]
13. Sun, S.; Bai, J.; Gu, J.; Guo, K.; Morley, N.; Gao, Q.; Zhang, Y.; Esling, C.; Zhao, X.; Zuo, L. Extraordinary mechanical properties and room-temperature magnetocaloric effects in spark plasma sintered all-d-metal Ni-Co-Mn-Ti alloy. *J. Alloys Compd.* **2024**, *976*, 173406. [CrossRef]
14. Wei, Z.Y.; Liu, E.K.; Chen, J.H.; Li, Y.; Liu, G.D.; Luo, H.Z.; Xi, X.K.; Zhang, H.W.; Wang, W.H.; Wu, G.H. Realization of multifunctional shape-memory ferromagnets in all-*d*-metal Heusler phases. *Appl. Phys. Lett.* **2015**, *107*, 022406. [CrossRef]
15. Wei, Z.Y.; Liu, E.K.; Li, Y.; Han, X.L.; Du, Z.W.; Luo, H.Z.; Liu, G.D.; Xi, X.K.; Zhang, H.W.; Wang, W.H.; et al. Magnetostructural martensitic transformations with large volume changes and magneto-strains in all-*d*-metal Heusler alloys. *Appl. Phys. Lett.* **2016**, *109*, 071904. [CrossRef]
16. Bez, H.N.; Pathak, A.K.; Biswas, A.; Zarkevich, N.; Balema, V.; Mudryk, Y.; Johnson, D.D.; Pecharsky, V.K. Giant enhancement of the magnetocaloric response in Ni–Co–Mn–Ti by rapid solidification. *Acta Mater.* **2019**, *173*, 225–230. [CrossRef]
17. Li, Y.; Qin, L.; Zhang, H.; Li, L. Tailored martensitic transformation and enhanced magnetocaloric effect in all-d-metal $Ni_{35}Co_{15}Mn_{33}Fe_2Ti_{15}$ alloy ribbons. *Chin. Phys. B* **2022**, *31*, 087103. [CrossRef]
18. Zhang, F.; Westra, K.; Shen, Q.; Batashev, I.; Kiecana, A.; van Dijk, N.; Brück, E. The second-order magnetic phase transition and magnetocaloric effect in all-d-metal NiCoMnTi-based Heusler alloys. *J. Alloy Compd.* **2022**, *906*, 164337. [CrossRef]
19. Samanta, S.; Chatterjee, S.; Sinha, J.; Mandal, K. Giant reversibility of magnetoresponsive properties in all- d -metal Ni-Co-Mn(Cu)-Ti Heusler alloys: Role of phase-fraction-assisted magnetostructural transition. *Phys. Rev. Mater.* **2023**, *7*, 084406. [CrossRef]
20. Li, Y.; Ye, X.; Lou, L.; Wang, L.; Qin, L. Ferromagnetic Martensitic Transition and Magnetocaloric Effect in $Ni_{35}Co_{15-x}V_xMn_{35}Ti_{15}$ (x = 1, 2, 3) All-d-Metal Heusler Alloy Ribbons. *J. Supercond. Nov. Magn.* **2023**, *36*, 1–6. [CrossRef]
21. Khan, A.N.; Moreno-Ramírez, L.M.; Díaz-García, Á.; Law, J.Y.; Franco, V. All-d-metal Ni(Co)-Mn(X)-Ti (x = Fe or Cr) Heusler alloys: Enhanced magnetocaloric effect for moderate magnetic fields. *J. Alloy Compd.* **2023**, *931*, 167559. [CrossRef]
22. Zhang, F.; Batashev, I.; van Dijk, N.; Brück, E. Reduced Hysteresis and Enhanced Giant Magnetocaloric Effect in B-Doped all-*d*-Metal Ni-Co-Mn-Ti-Based Heusler Materials. *Phys. Rev. Appl.* **2022**, *17*, 054032. [CrossRef]
23. Luo, H.; Meng, F.; Jiang, Q.; Liu, H.; Liu, E.; Wu, G.; Wang, Y. Effect of boron on the martensitic transformation and magnetic properties of $Ni_{50}Mn_{36.5}Sb_{13.5-x}B_x$ alloys. *Scr. Mater.* **2010**, *63*, 569–572. [CrossRef]
24. Pandey, S.; Quetz, A.; Rodionov, I.D.; Aryal, A.; Blinov, M.I.; Titov, I.S.; Prudnikov, V.N.; Granovsky, A.B.; Dubenko, I.; Stadler, S.; et al. Magnetic, transport, and magnetocaloric properties of boron doped Ni-Mn-In alloys. *J. Appl. Phys.* **2015**, *117*, 183905. [CrossRef]
25. Meng, F.; Hao, H.; Liu, X.; Luo, H. Effect of B doping on phase transition and magnetic properties of $Mn_{50}Ni_{40}In_{10-x}B_x$: Experimental and theoretical investigation. *J. Phys. Chem. Solids* **2018**, *123*, 19–24. [CrossRef]
26. Cicek, M.; Saritas, S.; Yildirim, O.; Emre, B. Effect of the low constituent boron on martensitic transformation, magnetic, and magnetocaloric properties of $Ni_{50}Mn_{35}In_{15}$ Heusler alloys. *J. Alloy Compd.* **2020**, *845*, 155493. [CrossRef]
27. Li, Y.; Huang, S.; Wang, W.; Liu, E.; Li, L. Ferromagnetic martensitic transformation and large magnetocaloric effect in $Ni_{35}Co_{15-x}Fe_xMn_{35}Ti_{15}$ (x = 2, 4, 6, 8) alloys. *J. Appl. Phys.* **2020**, *127*, 233907. [CrossRef]

28. López-Cruz, M.; Zamora, J.; Sánchez-Valdés, C.F.; Llamazares, J.L.S. On the synthesis, structural transformation and magnetocaloric behavior of $Ni_{37.5}Co_{12.5}Mn_{35}Ti_{15}$ melt-spun ribbons. *AIP Adv.* **2021**, *11*, 015010. [CrossRef]
29. Bez, H.N.; Yibole, H.; Pathak, A.; Mudryk, Y.; Pecharsky, V. Best practices in evaluation of the magnetocaloric effect from bulk magnetization measurements. *J. Magn. Magn. Mater.* **2018**, *458*, 301–309. [CrossRef]
30. Da, S.; Zheng, Z.; Huang, P.; Qiu, Z.; Zeng, D. Effect of B doping on magnetic and mechanical properties of all-d-metal Heusler alloys. *Phys. B Condens. Matter* **2023**, *670*, 415396. [CrossRef]
31. Gorria, P.; Llamazares, J.L.S.; Álvarez, P.; Pérez, M.J.; Marcos, J.S.; Blanco, J.A. Relative cooling power enhancement in magnetocaloric nanostructured Pr_2Fe_{17}. *J. Phys. D Appl. Phys.* **2008**, *41*, 192003. [CrossRef]

Disclaimer/Publisher's Note: The statements, opinions and data contained in all publications are solely those of the individual author(s) and contributor(s) and not of MDPI and/or the editor(s). MDPI and/or the editor(s) disclaim responsibility for any injury to people or property resulting from any ideas, methods, instructions or products referred to in the content.